CLEO CONF 96-19
ICHEP96 PA05-114

Measurement of the Branching Ratios for the Decays of D_s^+ to $\eta\pi^+$, $\eta'\pi^+$, $\eta\rho^+$, and $\eta'\rho^+$

CLEO Collaboration

(July 23, 1996)

Abstract

Using a data sample with integrated luminosity of about 3.6 fb^{-1} collected with the CLEO-II detector at the Cornell Electron Storage Ring, we have measured the branching ratios for the decay modes $D_s^+ \to (\eta, \eta')\pi^+$ and $D_s^+ \to (\eta, \eta')\rho^+$ relative to the standard normalization mode, $D_s^+ \to \phi\pi^+$. These decay modes are among the most common hadronic decays of the D_s^+, and can be related by factorization to the semileptonic decays $D_s^+ \to (\eta, \eta')\ell^+\nu$. The results obtained are compared with previous CLEO results on the same hadronic modes and with the branching ratios measured for the related semileptonic decays.

J. Bartelt,[1] S. E. Csorna,[1] V. Jain,[1] S. Marka,[1] A. Freyberger,[2] R. Godang,[2] D. Gibaut,[2] K. Kinoshita,[2] I. C. Lai,[2] P. Pomianowski,[2] S. Schrenk,[2] G. Bonvicini,[3] D. Cinabro,[3] L. Perera,[3] B. Barish,[4] M. Chadha,[4] S. Chan,[4] G. Eigen,[4] J. S. Miller,[4] C. O'Grady,[4] M. Schmidtler,[4] J. Urheim,[4] A. J. Weinstein,[4] F. Würthwein,[4] D. M. Asner,[5] D. W. Bliss,[5] W. S. Brower,[5] G. Masek,[5] H. P. Paar,[5] J. Gronberg,[6] C. M. Korte,[6] D. J. Lange,[6] R. Kutschke,[6] S. Menary,[6] R. J. Morrison,[6] S. Nakanishi,[6] H. N. Nelson,[6] T. K. Nelson,[6] C. Qiao,[6] J. D. Richman,[6] D. Roberts,[6] A. Ryd,[6] H. Tajima,[6] M. S. Witherell,[6] R. Balest,[7] B. H. Behrens,[7] K. Cho,[7] W. T. Ford,[7] H. Park,[7] P. Rankin,[7] J. Roy,[7] J. G. Smith,[7] J. P. Alexander,[8] C. Bebek,[8] B. E. Berger,[8] K. Berkelman,[8] K. Bloom,[8] D. G. Cassel,[8] H. A. Cho,[8] D. M. Coffman,[8] D. S. Crowcroft,[8] M. Dickson,[8] P. S. Drell,[8] R. Ehrlich,[8] R. Elia,[8] A. D. Foland,[8] P. Gaidarev,[8] B. Gittelman,[8] S. W. Gray,[8] D. L. Hartill,[8] B. K. Heltsley,[8] P. I. Hopman,[8] S. L. Jones,[8] J. Kandaswamy,[8] N. Katayama,[8] P. C. Kim,[8] D. L. Kreinick,[8] T. Lee,[8] Y. Liu,[8] G. S. Ludwig,[8] J. Masui,[8] J. Mevissen,[8] N. B. Mistry,[8] C. R. Ng,[8] E. Nordberg,[8] M. Ogg,[8,*] J. R. Patterson,[8] D. Peterson,[8] D. Riley,[8] A. Soffer,[8] C. Ward,[8] P. Avery,[9] M. Athanas,[9] C. D. Jones,[9] M. Lohner,[9] C. Prescott,[9] S. Yang,[9] J. Yelton,[9] J. Zheng,[9] G. Brandenburg,[10] R. A. Briere,[10] D. Y.-J. Kim,[10] T. Liu,[10] M. Saulnier,[10] R. Wilson,[10] H. Yamamoto,[10] T. E. Browder,[11] F. Li,[11] Y. Li,[11] J. L. Rodriguez,[11] T. Bergfeld,[12] B. I. Eisenstein,[12] J. Ernst,[12] G. E. Gladding,[12] G. D. Gollin,[12] E. Johnson,[12] I. Karliner,[12] M. Palmer,[12] M. Selen,[12] J. J. Thaler,[12] K. W. Edwards,[13] A. Bellerive,[14] D. I. Britton,[14] R. Janicek,[14] D. B. MacFarlane,[14] K. W. McLean,[14] P. M. Patel,[14] A. J. Sadoff,[15] R. Ammar,[16] P. Baringer,[16] A. Bean,[16] D. Besson,[16] D. Coppage,[16] C. Darling,[16] R. Davis,[16] N. Hancock,[16] S. Kotov,[16] I. Kravchenko,[16] N. Kwak,[16] S. Anderson,[17] Y. Kubota,[17] M. Lattery,[17] J. J. O'Neill,[17] S. Patton,[17] R. Poling,[17] T. Riehle,[17] A. Smith,[17] V. Savinov,[17] M. S. Alam,[18] S. B. Athar,[18] Z. Ling,[18] A. H. Mahmood,[18] H. Severini,[18] S. Timm,[18] F. Wappler,[18] A. Anastassov,[19] S. Blinov,[19,†] J. E. Duboscq,[19] R. Fulton,[19] D. Fujino,[19] K. K. Gan,[19] T. Hart,[19] K. Honscheid,[19] H. Kagan,[19] R. Kass,[19] J. Lee,[19] M. Sung,[19] A. Undrus,[19,†] R. Wanke,[19] A. Wolf,[19] M. M. Zoeller,[19] B. Nemati,[20] S. J. Richichi,[20] W. R. Ross,[20] P. Skubic,[20] M. Wood,[20] M. Bishai,[21] J. Fast,[21] E. Gerndt,[21] J. W. Hinson,[21] D. H. Miller,[21] E. I. Shibata,[21] I. P. J. Shipsey,[21] M. Yurko,[21] L. Gibbons,[22] S. D. Johnson,[22] Y. Kwon,[22] S. Roberts,[22] E. H. Thorndike,[22] C. P. Jessop,[23] K. Lingel,[23] H. Marsiske,[23] M. L. Perl,[23] S. F. Schaffner,[23] D. Ugolini,[23] R. Wang,[23] X. Zhou,[23] T. E. Coan,[24] V. Fadeyev,[24] I. Korolkov,[24] Y. Maravin,[24] I. Narsky,[24] V. Shelkov,[24] R. Stroynowski,[24] J. Staeck,[24] I. Volobouev,[24] J. Ye,[24] M. Artuso,[25] A. Efimov,[25] M. Gao,[25] M. Goldberg,[25] R. Greene,[25] F. Frasconi,[25] D. He,[25] S. Kopp,[25] G. C. Moneti,[25] R. Mountain,[25] Y. Mukhin,[25] S. Schuh,[25] T. Skwarnicki,[25] S. Stone,[25] and X. Xing[25]

[1]Vanderbilt University, Nashville, Tennessee 37235
[2]Virginia Polytechnic Institute and State University, Blacksburg, Virginia 24061
[3]Wayne State University, Detroit, Michigan 48202

---

*Permanent address: University of Texas at Austin.

†Permanent address: BINP, RU-630090 Novosibirsk, Russia.

[4]California Institute of Technology, Pasadena, California 91125
[5]University of California, San Diego, La Jolla, California 92093
[6]University of California, Santa Barbara, California 93106
[7]University of Colorado, Boulder, Colorado 80309-0390
[8]Cornell University, Ithaca, New York 14853
[9]University of Florida, Gainesville, Florida 32611
[10]Harvard University, Cambridge, Massachusetts 02138
[11]University of Hawaii at Manoa, Honolulu, Hawaii 96822
[12]University of Illinois, Champaign-Urbana, Illinois 61801
[13]Carleton University, Ottawa, Ontario, Canada K1S 5B6
and the Institute of Particle Physics, Canada
[14]McGill University, Montréal, Québec, Canada H3A 2T8
and the Institute of Particle Physics, Canada
[15]Ithaca College, Ithaca, New York 14850
[16]University of Kansas, Lawrence, Kansas 66045
[17]University of Minnesota, Minneapolis, Minnesota 55455
[18]State University of New York at Albany, Albany, New York 12222
[19]Ohio State University, Columbus, Ohio 43210
[20]University of Oklahoma, Norman, Oklahoma 73019
[21]Purdue University, West Lafayette, Indiana 47907
[22]University of Rochester, Rochester, New York 14627
[23]Stanford Linear Accelerator Center, Stanford University, Stanford, California 94309
[24]Southern Methodist University, Dallas, Texas 75275
[25]Syracuse University, Syracuse, New York 13244

I. INTRODUCTION

Among the most common hadronic decay modes for the D_s^+ are the decays $D_s^+ \to (\eta,\eta')\pi^+$ and $D_s^+ \to (\eta,\eta')\rho^+$. (We use the notation $D_s^+ \to (\eta,\eta')\pi^+$ to represent the decays $D_s^+ \to \eta\pi^+$ and $D_s^+ \to \eta'\pi^+$.) As can be seen from Figure 1, they are related by factorization to the semileptonic decays $D_s^+ \to (\eta,\eta')\ell^+\nu$. This relation has been extensively discussed in a paper by Kamal, Xu, and Czarnecki [1].

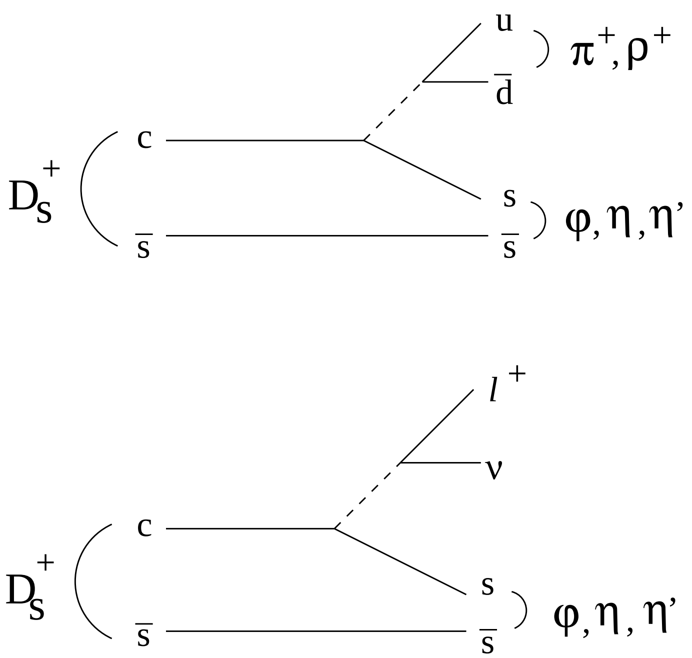

FIG. 1. Feynman digram of D_s^+ decays

One prediction of the factorization hypothesis is:

$$\Gamma(D_s^+ \to \eta\rho^+) = 6\pi^2 a_1^2 f_\rho^2 |V_{ud}|^2 \, \frac{d\Gamma}{dq^2}(D_s^+ \to \eta\ell^+\nu)|_{(q^2=m_\rho^2)}. \qquad (1)$$

Here f_ρ is the decay constant for the ρ and a_1 is a strong interaction coefficient that is measured in two-body hadronic D^0 decays.

To test the factorization prediction experimentally, a form for the shape of the form factor must be assumed. It should be very close to the form factor for $D^0 \to K^- e^+\nu$, for which

$$\frac{\Gamma(D^0 \to K^- e^+\nu)}{d\Gamma(D^0 \to K^- e^+\nu)/dq^2}_{(q^2=m_\rho^2)} = 1.30 \pm 0.01 \text{ GeV}^2.$$

This number is calculated using the CLEO measurement of the form factor [2]. Assuming a similar pole shape for the D_s^+ form factor yields the prediction $\Gamma(D_s^+ \to \eta\rho^+)/\Gamma(D_s^+ \to \eta\ell^+\nu) \approx 2.86$ and $\Gamma(D_s^+ \to \eta'\rho^+)/\Gamma(D_s^+ \to \eta'\ell^+\nu) \approx 2.86$ [1].

In 1992 CLEO [3] measured the branching ratios for the modes being studied here using a much smaller data sample of 689 pb^{-1}. Combining these measurements with CLEO measurements of the semileptonic modes [4], we calculate the $\Gamma(D_s^+ \to \eta\rho^+)/\Gamma(D_s^+ \to \eta\ell^+\nu) =$

4.3 ± 1.1 and $\Gamma(D_s^+ \to \eta'\rho^+)/\Gamma(D_s^+ \to \eta'\ell^+\nu) = 14.8\pm5.8$. The last number is well above the factorization prediction of 2.86. Theoretical efforts to understand charm nonleptonic decays, even including final state interactions, cannot account for the very large branching ratio for $D_s^+ \to \eta'\rho^+$ [5,6]. In this paper we used a 3.6 fb^{-1} data sample to remeasure the four modes, $D_s^+ \to (\eta,\eta')\pi^+$ and $D_s^+ \to (\eta,\eta')\rho^+$. The CLEO detector is described in Ref. [7].

II. EVENT SELECTION

All events in this analysis are required to pass standard CLEO criteria for hadronic events. No hadron identification is required, in order to reduce systematic errors. All D_s^+ candidates [1] are required to have $x = P_{D_s}/E_{beam} > 0.63$ to suppress combinatoric backgrounds.

All photons are required to be in the good barrel region of the calorimeter, to have a minimum energy of 30 MeV, and to not match the projection of a charged track. To select $\pi^0 \to \gamma\gamma$ decays, the $\gamma\gamma$ pairs are kinematically constrained to the nominal π^0 mass in order to improve the momentum resolution of the π^0 . We also require that $|\cos\theta_{\pi^0}| < 0.8$, where θ_{π^0} is the angle between one γ and the boost direction in the π^0 rest frame. This requirement reduces backgrounds from very soft photons.

For $\eta \to \gamma\gamma$ decays, the η is selected in a manner similar to the π^0, but with the additional constraint that photons which could be paired to make π^0s with momentum greater than 0.8 GeV/c are rejected. We also detect η's using the $\eta \to \pi^+\pi^-\pi^0$ decay chain. Generally this gives a sample with fewer events and less significance than for the other η decay mode. For the three-pion decay, the π^0 momentum is required to be greater than 0.4 GeV/c. All η candidates within 2.5 $\sigma(M)$ of the nominal mass are considered, where $\sigma(M)$ is the rms mass resolution for the given mode, typically about 14 MeV for the $\gamma\gamma$ mode, and 6 MeV for the $\pi^+\pi^-\pi^0$ mode. In order to improve the momentum resolution of the η, the decay particles from the η are kinematically constrained to the nominal η mass.

To select η' candidates we use the $\eta\pi^+\pi^-$ final state, where the η is detected in both $\gamma\gamma$ and $\pi^+\pi^-\pi^0$ modes. Both η and η' candidates are kinematically constrained to the nominal mass in order to improve the momentum resolution.

III. D_s^+ DECAYS INTO MODES CONTAINING A π^+

Five modes are studied in which a pion is produced in the weak decay:

1. $D_s^+ \to \phi\pi^+$ (the normalization mode), $\phi \to K^+K^-$
2. $D_s^+ \to \eta\pi^+,\ \eta \to \gamma\gamma$
3. $D_s^+ \to \eta\pi^+,\ \eta \to \pi^+\pi^-\pi^0$
4. $D_s^+ \to \eta'\pi^+,\ \eta' \to \eta\pi^+\pi^-,\ \eta \to \gamma\gamma$

---

[1] Throughout this paper, reference to a particular charge state implies the inclusion of the charge-conjugate state as well.

5. $D_s^+ \to \eta' \pi^+,\ \eta' \to \eta \pi^+ \pi^-,\ \eta \to \pi^+ \pi^- \pi^0$

We require the pions that come directly from the weak decay to have momentum greater than 0.7 GeV/c and the η or η' from the D_s^+ to have momentum greater than 1 GeV/c. This reduces the backgrounds from random combinations.

A. $D_s^+ \to \phi \pi^+$

Since this decay involves a pseudoscalar meson decaying into a vector meson and a pseudoscalar π^+, the ϕ must be polarized in the helicity zero state. The signal follows a $\cos^2 \theta_{K^+}$ distribution while the background is flat in $\cos \theta_{K^+}$, where θ_{K^+} is the angle between the K^+ and the D_s^+ in the ϕ rest frame, as defined in Figure 2. We require $|\cos \theta_{K^+}| > 0.45$. We select ϕ mesons within ± 8 MeV of the peak mass, and form the $\phi\pi^+$ mass spectrum shown in Figure 3.

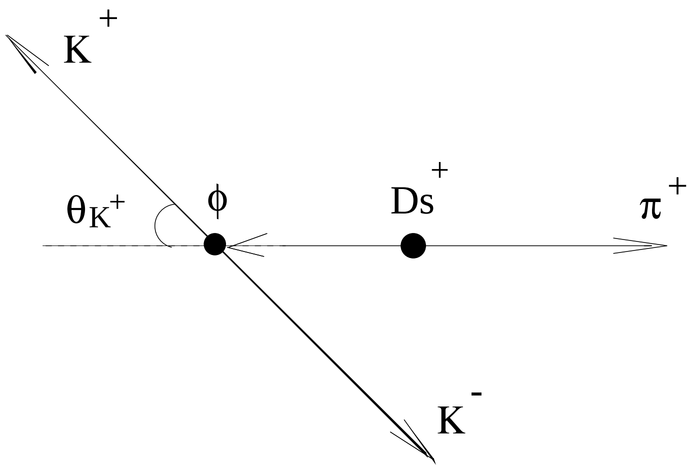

FIG. 2. Illustration of the helicity angle, θ_{K^+}. The D_s^+ decay is shown in its rest frame and the ϕ decay is drawn in its own rest frame.

The $\phi\pi^+$ mass distribution shows two clear peaks, one from the D_s^+ and the other from the D^+. To fit the spectrum we use four functions:

1. The D_s^+ signal shape comes from fitting signal peaks in Monte Carlo simulations to a double gaussian form. The central value is allowed to vary in the fit.

2. The D^+ signal shape is of the same form as for the D_s^+, with the mass constrained to be 0.099 GeV/c^2 less than the D_s^+ mass, which is the precisely measured mass difference [9].

3. A function to represent the $D_s^+ \to X\rho^+$ feed-through (X stands for ϕ, η, η') with shape determined by Monte Carlo and magnitude fixed from measurement [3]. This feed-through causes a broad peak centered around 1.7 GeV/c^2 when a π^0 from the ρ^+ is not reconstructed.

4. A Chebyshev polynomial is used to represent the combinatoric background.

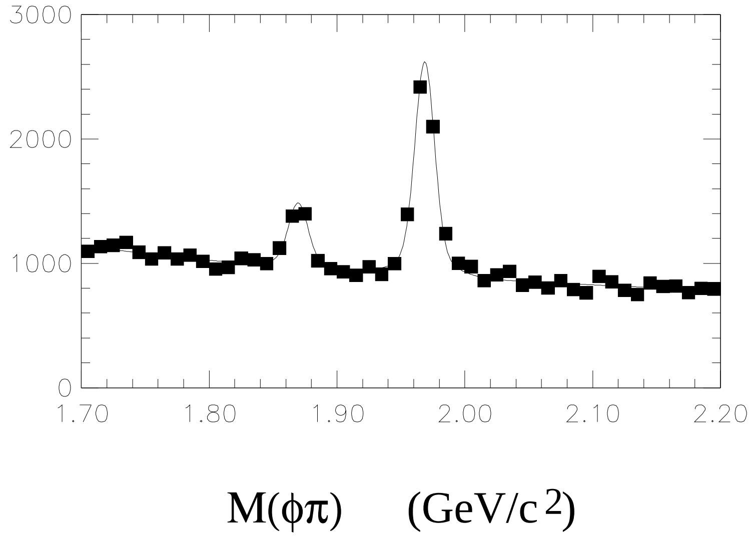

FIG. 3. D_s^+ mass spectrum for the decay $D_s^+ \to \phi\pi^+$. The smaller peak at lower mass is due to $D^+ \to \phi\pi^+$.

This fit yields 3748 ± 91 D_s^+ events. In all other fits, four functions are also used, although the combinatoric background shape depends on the particular mode.

B. $D_s^+ \to \eta\pi^+$

In Figure 4 we show the $\eta\pi^+$ invariant mass spectrum for both decay modes of the η. The signal peaks are evident for both the D_s^+ and D^+. The peak at the D_s^+ contains 766 ± 44 events for the channel $\eta \to \gamma\gamma$, and 154 ± 22 events for the channel $\eta \to \pi^+\pi^-\pi^0$. In Table I we list the yields for different channels and their efficiencies for D_s^+ decay. We also list the measurement for the ratio $\frac{\Gamma(D_s \to \eta_{\gamma\gamma}\pi)}{\Gamma(D_s \to \phi\pi)}$. In the table CL stands for confidence level; ϵ efficiency and ϵB, efficiency multiplied by branching fraction. The systematic errors for the efficiencies relative to the $\phi\pi$ mode have several sources and differ slightly from mode to mode. For the $\eta_{\gamma\gamma}\pi$ mode the systematic error includes uncertainties in the relative charged track (4%) and photon detection efficiencies (5%). We also studied the Monte-Carlo shape by letting the width of the two Gaussians float and then calculated the shift in the central value, giving us an uncertainty of 3%. We also used different background shapes to determine the uncertainty due to the unknown background shape, and obtained an error of 4%. The total systematic error obtained by adding these uncorrelated errors in quadrature is 8%.

The measured ratio for $\frac{\Gamma(D_s \to \eta_{3\pi}\pi)}{\Gamma(D_s \to \phi\pi)}$ shown in Table I is approximately 1.8 standard deviations lower than the corresponding ratio for the $\gamma\gamma$ mode. To calibrate the relative efficiency for these modes, we studied events of the type $D^{*+} \to D^0\pi^+$ and $D^0 \to \overline{K}^{*0}\eta$. This has a very large and clean signal, and an η momentum spectrum very similar to that for the D_s^+ decays. Using this process, we measure $B(\eta \to \gamma\gamma)/B(\eta \to \pi^+\pi^-\pi^0) = 1.53 \pm 0.16 \pm 0.10$, compared to the PDG value of 1.64 ± 0.04. This confirms that the relative efficiency for the two decay modes of the η is reproduced properly in the Monte Carlo simulation. We

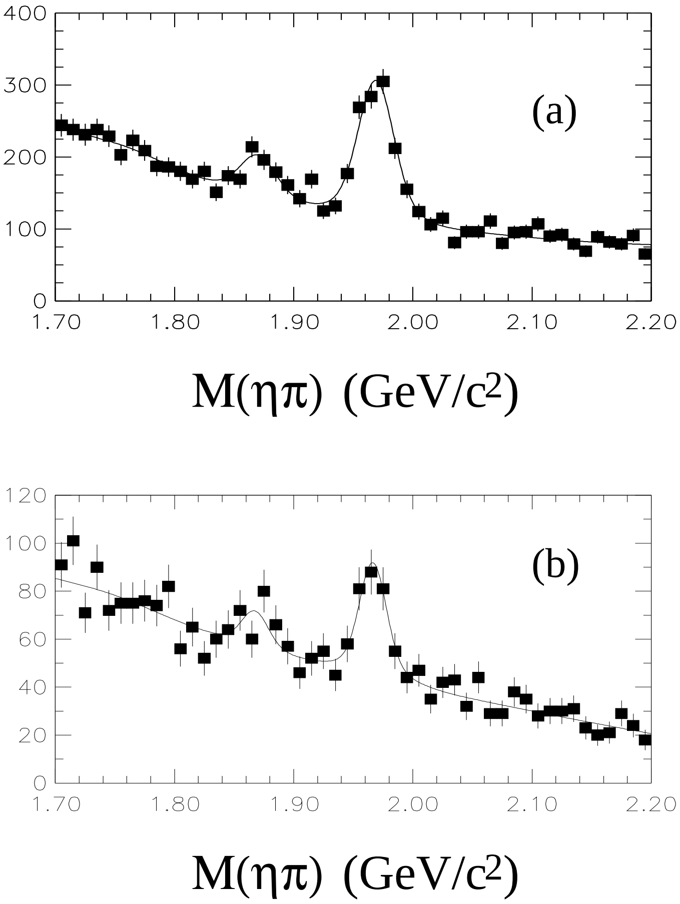

FIG. 4. D_s^+ mass spectrum of the decay channel $D_s^+ \to \eta\pi^+$ for (a) $\eta \to \gamma\gamma$, (b) $\eta \to \pi^+\pi^-\pi^0$.

attribute the 1.8 standard deviation difference between the two $D_s^+ \to \eta\pi^+$ measurements to statistical fluctuations.

C. $D_s^+ \to \eta'\pi^+$

For this mode, we can apply cuts on both the η mass and the η' mass, reducing the background substantially. Each mass provides a kinematic constraint, helping to improve the resolution for the $\eta'\pi^+$ mass. As a result, these modes are significantly cleaner than $D_s^+ \to \eta\pi^+$. We also require the momentum of the η' to be greater than 1.0 GeV/c.

In Figure 5 we show the $\eta'\pi^+$ invariant mass spectrum for both η decay modes. The peak at the D_s^+ mass contains 479 ± 26 events for the channel $\eta \to \gamma\gamma$, and 58 ± 9 events for the channel $\eta \to \pi^+\pi^-\pi^0$. The efficiencies and relative branching ratios are shown in Table I. The systematic error on the $\eta \to \gamma\gamma$ measurement due to the charged track efficiency is negligible compared to other errors since $\eta' \to \eta\pi^+\pi^-$ has the same number of tracks as $\phi \to K^+K^-$. The main contributions to the systematic error are the uncertainties

TABLE I. Fit Results for $D_s^+ \to (\eta, \eta')\pi^+$

Type	N	CL(%)	ϵ(%)	ϵB(%)	$\Gamma/\Gamma(\phi\pi)$
$\phi\pi$	3748 ± 91	0.08	19.1 ± 0.2	9.4	
$\eta_{\gamma\gamma}\pi$	766 ± 44	39.6	9.6 ± 0.1	3.7	$0.52 \pm 0.03 \pm 0.04$
$\eta_{3\pi}\pi$	154 ± 22	83.8	4.5 ± 0.1	1.1	$0.35 \pm 0.05 \pm 0.06$
$\eta'(\eta_{\gamma\gamma})\pi$	479 ± 26	1.5	6.7 ± 0.1	1.1	$1.09 \pm 0.06 \pm 0.07$
$\eta'(\eta_{3\pi})\pi$	58 ± 9	10.8	1.9 ± 0.1	0.2	$0.73 \pm 0.11 \pm 0.12$

in the photon detection efficiency (5%), the uncertainties in the signal shape (3%) and the uncertainties in the background shape (3%). The total systematic error obtained by adding these uncorrelated errors in quadrature is 6%.

In ${D_s}^+ \to \eta'\pi^+$, $\eta' \to \eta\pi^+\pi^-$, $\eta \to \pi^+\pi^-\pi^0$, we found that there are many events with multiple combinations of pions which satisfy our selection criteria. Most of them come from real η' decays in which different rearrangements of the same four charged pions (two directly from the η' and two from the η), plus the π^0, pass our η and η' cuts. We take only one candidate per event, choosing the candidate with the minimum value of a χ^2 based on the π^0, η, and η' masses ($\chi^2 = \frac{(\delta M_{\eta'})^2}{\sigma^2_{\eta'}} + \frac{(\delta M_\eta)^2}{\sigma^2_\eta} + \frac{(\delta M_{\pi^0})^2}{\sigma^2_{\pi^0}}$). The resulting measurement is shown in Table I.

IV. D_s^+ DECAYS INTO MODES CONTAINING A ρ^+

For the decays with a ρ^+ in the final state, most cuts are very similar to those for the analogous channel with the ρ^+ replaced by a π^+. Because of lower rates, lower efficiency, and a serious problem with multiple combinations from the same event, the $\eta \to \pi^+\pi^-\pi^0$ decay does not add significantly to the measurements of these modes, and is not used.

A. $D_s^+ \to \eta\rho^+$

For the decay mode $D_s^+ \to \eta\rho^+$, we require the helicity angle to be in the range $|\cos\theta_{\pi^+}| > 0.45$, and the invariant mass of the $\pi^+\pi^0$ to be within ± 170 MeV$/c^2$ of the ρ^+ mass. The resulting $\eta\pi^+\pi^0$ mass spectra is shown in Figure 6, yielding 589 ± 43 $D_s^+ \to \eta\pi^+\pi^0$ events. The relative branching ratio derived from this yield is $\Gamma(D_s^+ \to \eta_{\gamma\gamma}\pi^+\pi^0)/\Gamma(D_s^+ \to \phi\pi^+) = 3.29 \pm 0.24$. We cannot directly interpret this as a branching ratio for $D_s^+ \to \eta\rho^+$, however, until we account for possible nonresonant feedthrough.

Although cuts on the helicity angle and on the ρ mass region can be used, the most reliable way to measure the resonant branching ratio is to fit the Dalitz plot. By doing this we make full use of the di-pion mass and the helicity angle to separate the $\eta\rho^+$ signal. We therefore make a Dalitz plot of all events with $1.94 < M(\eta\pi^+\pi^0) < 1.99$ GeV$/c^2$, removing the cuts on helicity angle and on the $\pi^+\pi^0$ mass. In Figure 7 we show four Dalitz plots:

a) The signal region in the data, defined as $1.94 < M(\eta\pi^+\pi^0) < 1.99$ GeV$/c^2$.

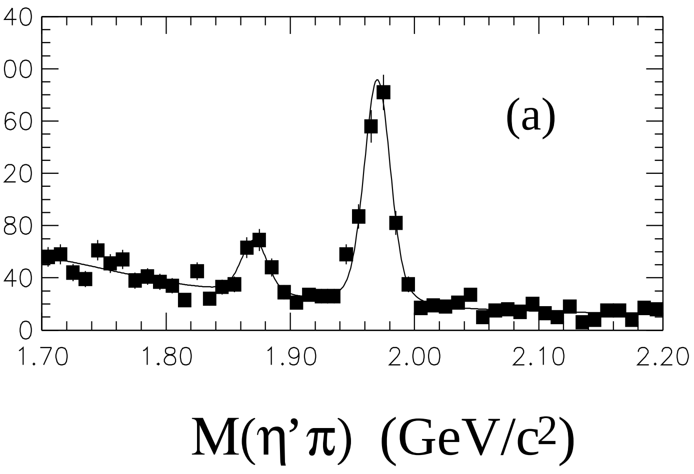

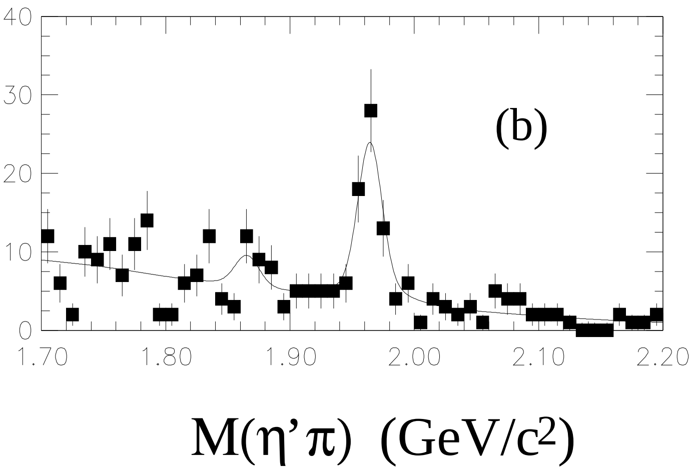

FIG. 5. D_s^+ mass spectrum of the decay channel $D_s^+ \to \eta'\pi^+$, $\eta' \to \eta\pi^+\pi^-$ for (a) $\eta \to \gamma\gamma$, (b) $\eta \to \pi^+\pi^-\pi^0$.

b) The M_{D_s} data sidebands. The sidebands are the mass regions $1.75 < M(\eta\pi^+\pi^0) < 1.90$ GeV/c^2 and $2.04 < M(\eta\pi^+\pi^0) < 2.24$ GeV/c^2.

c) The full Monte Carlo of the $\eta\rho^+$ signal.

d) A simulation using a parameterized Monte Carlo of nonresonant $\eta\pi^+\pi^0$ events generated according to phase space.

We do not expect $\eta\pi$ resonant structures in this Dalitz plot because isospin forbids $s\bar{s} \to \eta\pi$. For all four Dalitz plots, we recalculate the values of $M^2(\eta\pi^+)$ and $M^2(\pi^+\pi^0)$ so that the Dalitz boundary corresponds exactly to that of the D_s^+, giving the sidebands the same boundary as the signal region. This causes negligible smearing of the ρ^+ resonance.

The most obvious feature of the Dalitz plot is that the ρ^+ region stands out so clearly in the data, even though there is a significant background from the D_s^+ sidebands. We do a

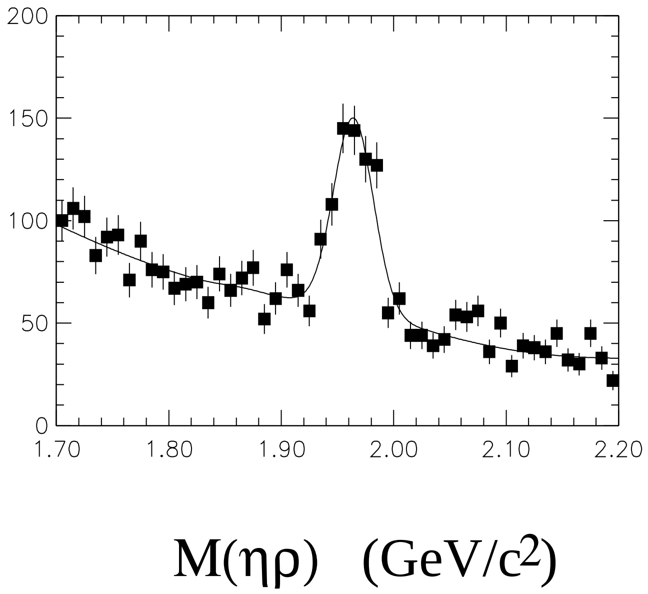

FIG. 6. D_s^+ mass spectrum of the decay channel $D_s^+ \to \eta\rho^+$, $\eta \to \gamma\gamma$.

binned Dalitz fit to the data distribution in the signal region using the sum of the distributions in the other three plots in Figure 7. The normalization of the non-D_s^+ component is fixed using a fit to the $\eta\rho^+$ mass distribution. The number of the resonant and nonresonant D_s^+ events is varied in the fit, with no interference term allowed. The results of the fit are shown in Table II. The systematic error includes uncertainties in the signal shape (4%), the relative efficiency for charged tracks (4%) and photons (10%), the background shape (3%), and the nonresonant shape and any possible interference of the signal with this shape (5%). The total systematic error, obtained by adding these uncorrelated errors in quadrature, is estimated to be 13%.

B. $D_s^+ \to \eta'\rho^+$

We search for $D_s^+ \to \eta'\rho^+$ only using the decay mode $\eta' \to \eta\pi^+\pi^-$, $\eta \to \gamma\gamma$. For the $\eta \to \pi^+\pi^-\pi^0$ decay, there are two soft π^0s and as a result too many wrong combinations to be useful. We require the momentum of the η' to be greater than 1.0 GeV/c and the invariant mass of the two pions to be within ±170 MeV of the ρ^+ mass. In Figure 8 we can see a clean peak of $M_{\eta'\pi^+\pi^0}$. The fit yields 181 ± 18 events.

The branching ratio derived from this number is $\Gamma(D_s^+ \to \eta'\pi^+\pi^0)/\ \Gamma(D_s^+ \to \phi\pi^+) = 2.98{\pm}0.30$. Again, we must be able to subtract the nonresonant feedthrough in this mode. A Dalitz plot is not as useful in separating signal from background, because the kinematic range for the di-pion mass does not extend beyond the region of the ρ. Again, we do not expect $\eta'\pi$ resonant structures in this Dalitz plot because isospin forbids $s\bar{s} \to \eta'\pi$. We therefore fit the angular distribution alone to extract the ρ component. As in the case of the Dalitz fit for $\eta\rho^+$, we use three components in the fit: (a) The resonant signal shape, a

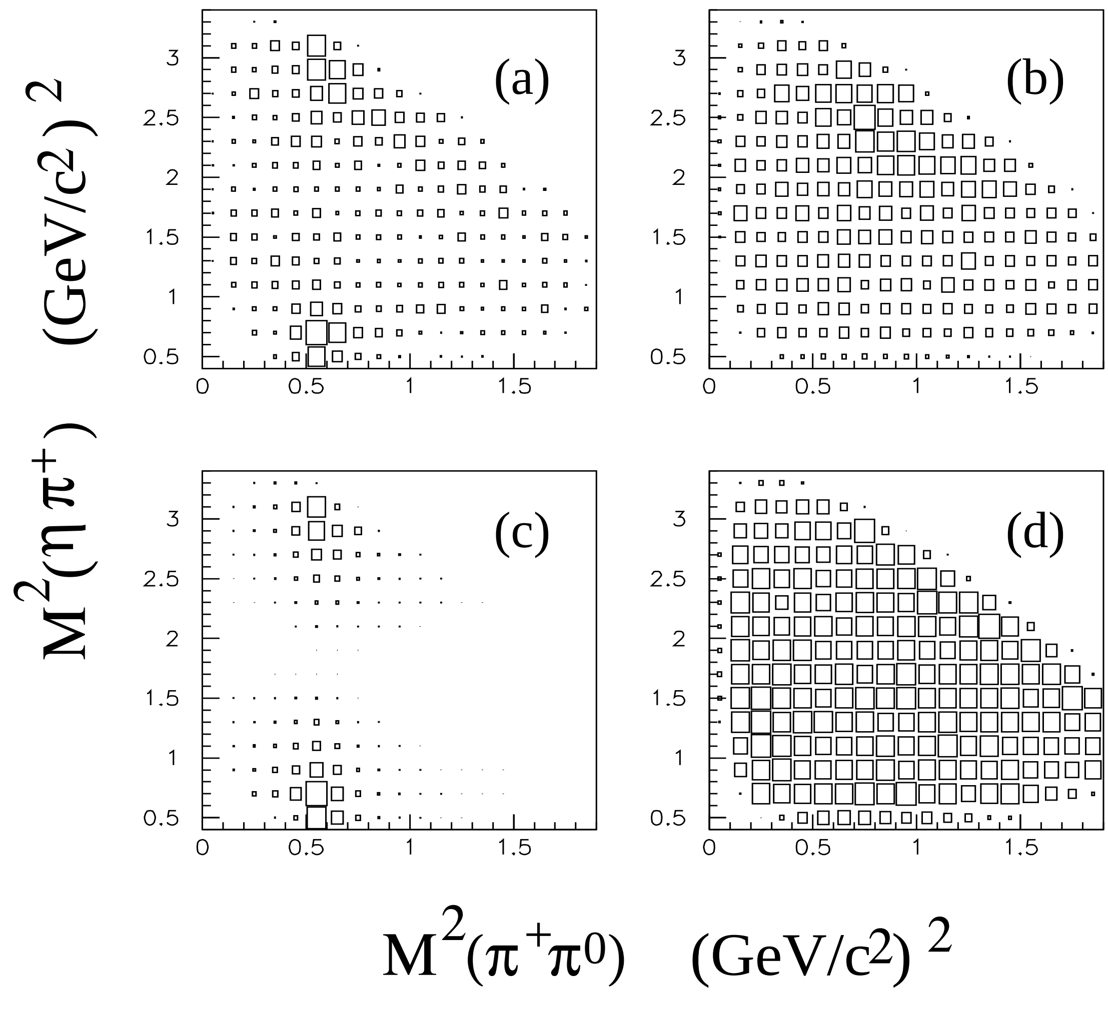

FIG. 7. Dalitz plot of $D_s^+ \to \eta\pi$, $\eta \to \gamma\gamma$. The horizontal axis is $M^2_{\pi^+\pi^0}$; the vertical axis is $M^2_{\eta\pi^+}$. (a) Data signal region; (b) Data M_{D_s} sidebands; (c) MC signal; (d) MC simulation of nonresonant $\eta\pi^+\pi^0$ (generated according to phase space).

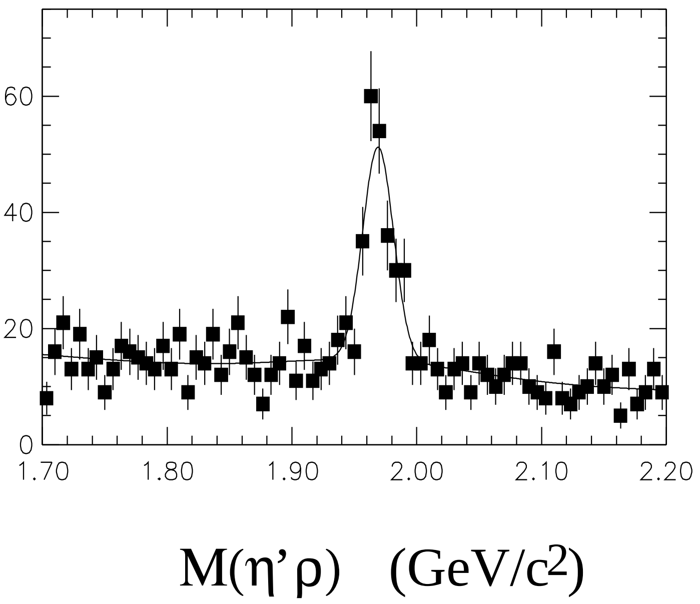

FIG. 8. D_s^+ mass spectrum of decay channel $D_s^+ \to \eta' \rho^+$.

fourth order polynomial determined from the Monte Carlo, which includes the distortion of the pure $\cos^2\theta$ shape due to detector acceptance; (b) a nonresonant D_s^+ shape, which is a straight line; (c) a non-D_s^+ background shape, a first order polynomial determined by fitting the sidebands. As for the Dalitz fit, we fix the background normalization from the D_s^+ mass fit, and vary the normalizations of the signal and nonresonant parts.

Figure 9 shows the fit of the helicity angle distribution for the events in the D_s^+ mass peak. The results of the fit are shown in Table II. The total systematic error is obtained by adding the photon detection efficiency error (10%) and uncertainties in the signal (4%), background (3%), and nonresonant (3%) shapes, for a total of 11%.

TABLE II. Fit Results for $D_s^+ \to (\eta, \eta')\rho^+$

Type	N	CL(%)	ϵ(%)	ϵB(%)	$\Gamma/\Gamma(\phi\pi)$
$\eta_{\gamma\gamma}\rho^+$	447 ± 31	57.5	1.82 ± 0.07	0.47	$2.98 \pm 0.20 \pm 0.39$
$\eta'(\eta_{\gamma\gamma})\rho^+$	137 ± 14	30.7	1.36 ± 0.04	0.155	$2.78 \pm 0.28 \pm 0.30$

V. CONCLUSION

We have remeasured the branching ratios of the two-body hadronic decays of the D_s^+, $D_s^+ \to (\eta, \eta')\pi^+$, and $D_s^+ \to (\eta, \eta')\rho^+$. The results are consistent with the old CLEO measurement [3], but have improved errors. Using weighted averages of the two η modes our results for $D_s^+ \to (\eta, \eta')\pi^+$ are:

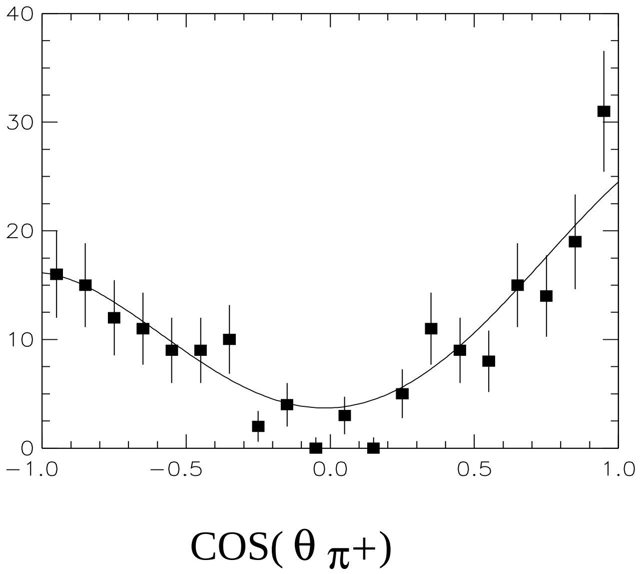

FIG. 9. The helicity angle distribution for the event in the D_s^+ mass peak of decay channel $D_s^+ \to \eta' \rho^+$, $\eta' \to \eta\pi^+\pi^-$, $\eta \to \gamma\gamma$.

$\frac{\Gamma(D_s^+ \to \eta\pi^+)}{\Gamma(D_s^+ \to \phi\pi^+)} = 0.47 \pm 0.03 \pm 0.06.$
$\frac{\Gamma(D_s^+ \to \eta'\pi^+)}{\Gamma(D_s^+ \to \phi\pi^+)} = 1.01 \pm 0.06 \pm 0.06,$
and the results for the ρ modes, taken from Table II, are:

$\frac{\Gamma(D_s^+ \to \eta\rho^+)}{\Gamma(D_s^+ \to \phi\pi^+)} = 2.98 \pm 0.20 \pm 0.39.$
$\frac{\Gamma(D_s^+ \to \eta'\rho^+)}{\Gamma(D_s^+ \to \phi\pi^+)} = 2.78 \pm 0.28 \pm 0.30.$

The improvement in the measurements comes mainly from the larger data sample. Using these measurements and CLEO semileptonic measurements [4] , we can calculate the ratios which test factorization: $\Gamma(D_s^+ \to \eta\rho^+)/\Gamma(D_s^+ \to \eta\ell^+\nu) = 4.4 \pm 1.2$ and $\Gamma(D_s^+ \to \eta'\rho^+)/\Gamma(D_s^+ \to \eta'\ell^+\nu) = 12.0 \pm 4.3$. The branching ratio for the mode $D_s^+ \to \eta'\rho^+$ is much larger than the value of 2.86 expected from factorization. Using the normalization $B(D_s^+ \to \phi\pi^+) = (3.5 \pm 0.4)\%$ [9], we calculate $B(D_s^+ \to \eta'\rho^+) = (9.7 \pm 1.8)\%$. This branching fraction is very large, considering the flavor wave function of the η' is only partly $s\bar{s}$ and that the rate is suppressed for such a P-wave decay very close to threshold. Models which explain other charm hadronic modes well predict $B(D_s^+ \to \eta'\rho^+)$ to be $1 - 3\%$ [5,6,8].

We gratefully acknowledge the effort of the CESR staff in providing us with excellent luminosity and running conditions. J.P.A., J.R.P., and I.P.J.S. thank the NYI program of the NSF, M.S thanks the PFF program of the NSF, G.E. thanks the Heisenberg Foundation, K.K.G., M.S., H.N.N., T.S., and H.Y. thank the OJI program of DOE, J.R.P, K.H., and M.S. thank the A.P. Sloan Foundation, and A.W., and R.W. thank the Alexander von Humboldt Stiftung for support. This work was supported by the National Science Foundation, the U.S. Department of Energy, and the Natural Sciences and Engineering Research Council of Canada.

REFERENCES

[1] A.N.Kamal *et al.*, Phys. Rev. D**49**, 1330 (1994).

[2] A. Bean *et al.* (CLEO), Phys. Lett. B**317**, 647 (1993).

[3] M.Daoudi *et al.* (CLEO), Phys. Rev. D**45**, 3965 (1992). The four measured branching ratios in that paper were: $\frac{\Gamma(D_s^+\to\eta\pi^+)}{\Gamma(D_s^+\to\phi\pi^+)} = 0.54\pm0.09\pm0.06$, $\frac{\Gamma(D_s^+\to\eta'\pi^+)}{\Gamma(D_s^+\to\phi\pi^+)} = 1.20\pm0.15\pm0.11$, $\frac{\Gamma(D_s^+\to\eta\rho^+)}{\Gamma(D_s^+\to\phi\pi^+)} = 2.86 \pm 0.38^{+0.36}_{-0.38}$, and $\frac{\Gamma(D_s^+\to\eta'\rho^+)}{\Gamma(D_s^+\to\phi\pi^+)} = 3.44 \pm 0.62^{+0.44}_{-0.46}$. The present paper includes the data used in the 1992 paper. Thus the newer results should not be averaged with the older results.

[4] G.Brandenburg *et al.* (CLEO), Phys. Rev. Letters **75**, 3804 (1995).

[5] I.Hinchliffe and T.A.Kaeding, Phys. Rev. D**54**, 914 (1996).

[6] F.Buccella *et al.*, Roma preprint 1-1130/96 (hep-ph/9601343) (1996).

[7] Y. Kubota *et al.* (CLEO), Nucl. Instrum. Methods Phys. Res., Sect. A **320**, 66 (1992).

[8] M. Bauer, B. Stech, and M. Wirbel, Z. Phys. C **34**, 102(1987).

[9] Particle Data Group, Phys. Rev.D **50**, 1(1994).